Ward, D.J., 2019, Dip, layer spacing, and incision rate controls on the formation of strike valleys, cuestas, and cliffbands in heterogeneous stratigraphy: Lithosphere, https://doi.org/10.1130/L1056.1.

GSA Data Repository Item 2019305

Data Repository Information

Numerical model description

We use a numerical landscape evolution model descended from the LEMming model of Ward et al. (2011). Numerically, it is a 2D, regular-grid finite difference model with D∞ flow routing and a cellular routine for rockfall. Experiments were all run on a 10-m raster grid using a dynamic timestep. We review the relevant features of the model here. The model is written in MATLAB and C, and the source code will be available from the Community Surface Dynamics Modeling System repository (http://csdms.colorado.edu) at the time of publication.

Drainage calculations

Channel slopes and contributing areas are calculated for each timestep using the D∞ algorithm of Tarboton (1997), which does not force flow from each pixel into only one neighboring pixel and thus does not artificially enhance or inhibit convergent or divergent flow, while remaining computationally efficient. The flow routing calculates drainage area, which is multiplied by a spatially uniform precipitation rate to yield a water discharge (*Q*). From discharge, stream velocity (*U*) is calculated using a Darcy-Weisbach relationship (Anderson and Anderson, 2010) and assuming a constant width-to-depth ratio (ϖ) of the stream cross-section:

$$U = \left(\frac{8gS\sqrt{\varpi Q}}{\varpi f}\right)^{2/5}, \qquad \text{(S1)}$$

where g is the gravitational acceleration, and S is channel slope. f=0.4 is the Darcy friction factor, here chosen to give ~1 m/s flow for a 50-cm-deep channel at a slope of 0.01. Stream width (*W*) and depth (*D*) are then calculated as

$$W = \sqrt{\varpi Q/U} \qquad \text{(S2)}$$

$$D = \frac{Q}{UW}. \qquad \text{(S3)}$$

This formulation allows velocity and depth to covary such that width and depth decrease with slope and velocity increases (e.g., Finnegan et al. 2005). Fluvial erosion ($\dot{E}$) is modeled as proportional to unit stream power (Ω) and is detachment-limited:

$$\dot{E} = k\Omega \qquad \text{(S4)}$$

$$\Omega = \tau U/W \qquad \text{(S5)}$$

$$\tau = \rho g D \sin(\tan^{-1} S), \qquad \text{(S6)}$$

where τ is the fluvial basal shear stress and ρ is the density of water. In practice, in our model, this fluvial erosion treatment behaves as if erosion is proportional to $A^m S^n$, with m/n = 0.5 (Fig. S1).

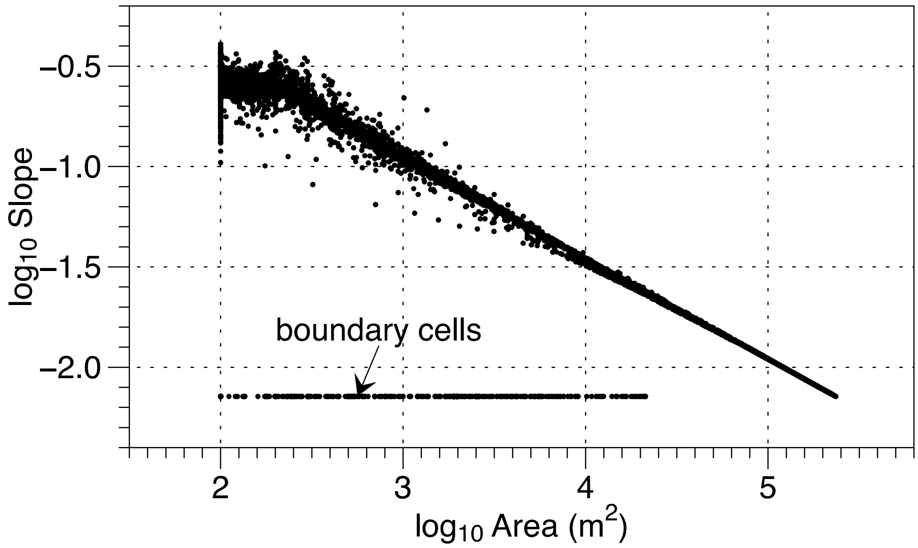

Fig. S1. Slope-area plot from the landscape model at near-steady state (uplift rate of 0.1 mm/yr) with uniform rock erodibility. Corresponds to the landscape of Section 4, main text, and movies SM1 to SM3, prior to cliff emergence.

Hillslopes

Here we use linear-diffusive erosion of hillslopes (Tucker and Bras, 1998). Apart from the rockfall debris, mobile regolith is not tracked; the landscape is assumed to be detachment-limited. As parameterized here, erosion is dominated by the fluvial and rockfall processes, and so the results are not sensitive to hillslope erosion parameters.

Rockfall

We detect viable rockfall source pixels by a slope-threshold and rocktype criterion, and 'fail' these pixels one by one at random until no more sources meet the failure criterion. This allows the rockfall rate to adjust to topographic changes dynamically. The slope threshold can vary between rocktypes, and we can turn off rockfall entirely on some rocktypes by setting the slope threshold to infinity. When a pixel 'fails' it is reduced in elevation to that of its highest downhill neighbor. Because the model cellsize is larger than most rockfall events in our field settings, and material can only be removed in the *x*,*y* directions in single-pixel increments, each pixel failure represents an amalgam of many 'real-life' rockfall events. This renders the process cellsize-dependent, because with larger pixels, there is more debris generated from each event and a longer waiting time between events. The long-term average amount of debris delivered per time is the same, however; the cellsize dependence is only in the distribution of event sizes. We mitigate this effect by performing our experiments at a standard grid spacing of 10 m throughout, similar to the major fracture spacing in the Ferron Sandstone (Sheehan and Ward, 2018), and within the range of typical large rockfall events in our field areas (Ward et al., 2011). Having calculated a volume of rockfall $dx \times dy \times H_f$, where H_f is the failure height, rockfall debris is spread across the landscape according to an angle-of-repose scheme.

The angle of repose algorithm is derived from a snow avalanching routine as implemented by Kessler et al. (2006). It calculates for each cell the topographic gradient in each direction ($x+$,$x-$,$y+$,$y-$) relative to the surrounding cells. Where this is steeper than the angle of repose, the elevation change needed to reduce the gradient to the angle of repose is computed. 1/3 of this difference is subtracted from the higher cell, and the same amount added to the lower cell. The process is iterated until the gradient is everywhere within a small tolerance of the angle of repose; usually only 2-3 iterations are needed. The algorithm is efficient in that each iteration can be applied across an entire grid at once, and areas of material not involved in the redistribution can be masked off and excluded.

In addition to redistribution, rockfall debris erodes by fluvial and hillslope processes over time. Its erodibility parameters are defined the same way as the other rocktypes in the model.

Stratigraphy

An arbitrary number of different stratigraphic units can be inserted in the model. Dipping stratigraphy is constructed functionally from overlapping rectilinear layers, whose minimum dimension in the x,y plane is one grid cell, and whose vertical dimension can be arbitrary. Erodibility is defined by the coefficients of the stream-power rule and the hillslope regolith diffusivity; these are defined independently as a list of ‘rock types’ and each stratigraphic unit is assigned the desired rock type from this list. Where the topographic surface intersects a stratigraphic unit, each property grid representing an erosion rule coefficient is set to the properties of the corresponding rock type. In the caprock, both the hillslope diffusivity and the stream power coefficient are set very low in order to limit fluvial erosion at the low slopes of the upper surface and promote formation of very steep slopes at the clifftop.

Model setup

Table ST1 contains the base parameterization used across model runs. Domain configurations and boundary conditions are described in the main text. We use a standard initial condition based on a synthetic landscape generated externally to the model. The initial condition for all runs is identical down to the random noise. Random noise is generated at the cellular scale then progressively filtered over wider and wider windows, so that random topographic perturbations occur at every horizontal scale between 20 cells (here, 200 m) and one cell (10 m).

In the cliff-retreat model runs, eventual exhumation of the down dip edge of the caprock results in rapid erosion of the backscarp and dissection of the caprock; this occurs more rapidly with higher uplift rates, so longer model domains are required for those runs.

Of the various model parameters, the retreat proportionality constant c_1 is primarily a function of the specified angle of initiation for the rockfall process (Fig. S2), and of the rockfall debris resistance to erosion (Ward and Sheehan, 2015). Different models with different rules for e.g. fluvial erosion, or different grid sizes or numerical schemes would almost certainly result in different values for c_1 (Eq. 3) and perhaps even for the form of the retreat rate-height relationship. We have not explored this parameter space here, but as noted in the main text, the key behavior depends only on a monotonic relationship between retreat rate and escarpment height.

Table ST1 - Numerical model base parameters and values

Parameter	Value	Unit	Description
Grid size			
x	125-240	pixels	Landscape size (X), depending on experiment (see text)
y	200-1000	pixels	Landscape size (Y), depending on experiment (see text)
dx	10	m	Grid cell size
dy	dx		
Timesteps and model duration			
dt	0.01-1000	yr	Timestep dynamic range
tmax	1.0E+07	yr	Model run duration
Physical parameters			
g	9.82	m/s^2	Gravitational acceleration
rho_w	1000	kg/m^3	Density of water
rho_rock	2700	kg/m^3	Density of rock
rho_reg	1500	kg/m^3	Density of regolith/rockfall debris
DepoAngleCutoff	25	º	Angle of repose for rockfall debris
Parameters for the channel geometry			
stream_WDR	10	-	Dimensionless stream width-to-depth ratio
f	0.4	-	Darcy-Weisbach friction factor
RRateMean	1	m/yr	Precipitation rate
Rocktype 0 - default substrate			
k0	5.0E-04	1/(m•yr)	Fluvial erodibility
kappa	1.0E-03	m^2/yr	Hillslope diffusivity
rfslope0	inf	m/m	Slope above which qualifies a rockfall source ("threshold slope")
Rocktype 1 - caprock			
k1	2.5E-06	1/(m•yr)	Fluvial erodibility
kappa1	1.0E-04	m^2/yr	Hillslope diffusivity
rfslope1	1.7	m/m	Slope above which qualifies a rockfall source ("threshold slope")
Rocktype 2 - rockfall debris			
k2	2.5E-04	1/(m•yr)	Fluvial erodibility

kappa2	5.0E-04	m^2/yr	Hillslope diffusivity
rfslope2	inf	m/m	Slope above which qualifies a rockfall source ("threshold slope")

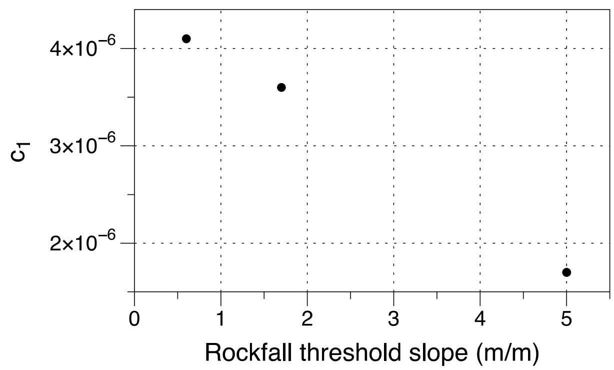

Fig. S2: Height-retreat proportionality constant c_1 exhibits a near-linear dependence on rockfall threshold angle.

Captions for supplemental media

Movie SM1. Model output movie of the two-caprock, step-change uplift rate scenario described in Section 4 of the main text. Erosion rates step from slow to fast, causing the escarpment to cross the H*=1 line (Fig. 4). Following this step, and a ~5 Ma period of somewhat complex transient adjustment, the escarpment has switched from a cuesta to a compound cliff.

Movie SM2. Model output movie of the two-caprock, variable uplift rate scenario described in Section 4 of the main text. Erosion rates average near the H*=1 line (Fig. 4); note the dynamic behavior with each uplift pulse, and the along-strike propagation of erosion waves when benches begin to form.

Movie SM2. Same as movie SM2, but with closed lateral boundaries and a “notch” of weaker rock that localizes a transverse stream in the middle of the model domain. The cliffs show the same behavior, illustrating independence from the model boundary conditions.

Supplement References

Anderson, R. S., and Anderson, S. P., 2010, Geomorphology: the mechanics and chemistry of landscapes: New York, Cambridge University Press.

Finnegan, N. J., Roe, G., Montgomery, D. R., and Hallet, B., 2005, Controls on the channel width of rivers: Implications for modeling fluvial incision of bedrock: Geology, v. 33, p. 229-232.

Kessler, M. A., Anderson, R. S., and Stock, G. M., 2006, Modeling topographic and climatic control of east-west asymmetry in Sierra Nevada glacier length during the Last Glacial Maximum: Journal of Geophysical Research: Earth Surface, v. 111(F2).

Sheehan, C. E., and Ward, D. J., 2018, Late Pleistocene talus flatiron formation below the Coal Cliffs cuesta, Utah, USA. Earth Surface Processes and Landforms.

Tarboton, D. G., 1997, A new method for the determination of flow directions and upslope areas in grid digital elevation models: Water resources research, v. 33, p. 309-319.

Tucker, G. E., and Bras, R. L., 1998, Hillslope processes, drainage density, and landscape morphology. Water Resources Research: v. 34, p. 2751-2764.

Ward, D. J., Berlin, M. M., and Anderson, R. S., 2011, Sediment dynamics below retreating cliffs. Earth Surface Processes and Landforms: v. 36, p. 1023-1043.

Ward, D., and Sheehan, C., 2015, December, Modeling the cliff retreat response to base-level change in layered rocks, Colorado Plateau, USA: Abstract EP53B-1024 presented at 2015 Fall Meeting, AGU, San Francisco, California, 14–18 December.